2011-01-0917

Sliding Mode Control of Air Path in Diesel-Dual-Fuel Engine

Withit Chatlatanagulchai and Ittidej Moonmangmee
Faculty of Engineering, Kasetsart University

Shinapat Rhienprayoon and Krisada Wannatong
PTT Research and Technology Institute, PTT Public Company Limited

ABSTRACT

In diesel-dual-fuel engine, CNG is injected at the intake ports and diesel fuel is injected at the cylinders. As a result of using CNG as main fuel, smaller amount of diesel is used mainly for ignition, resulting in lower fuel cost. However, stricter air path control is required because the engine now operates partly as a port fuel injection engine and partly as a diesel engine. As is evident from engine calibration, desired MAP and MAF have more abrupt change with wider range than those of diesel engine. In typical commercial truck, MAP and MAF are controlled separately using traditional controller such as PID with marginal control performance. Recently, more researchers have combined the control of MAP and MAF together as multivariable problem because both quantities reflect the behavior of the air path. In this paper, multivariable sliding mode control (SMC) is implemented in two-approaches, a model-reference-based and an integrator-augmented based. The diesel-dual-fuel engine was converted from a diesel engine and used in the engine test bed. Throttle and EGR valve were actuated to regulate MAP and MAF at their respective set points. Experimental results at an engine speed of 2000 rpm and 20% pedal showed that the two proposed algorithms delivered good tracking performance with fast action. The MAP and MAF responses were able to track their desired values with 2.5 seconds settling time and less than 10% overshoot. The integrator-augmented SMC had more response accuracy than the model-reference SMC but with more chattering.

INTRODUCTION

In countries where compressed natural gas (CNG) has lower price than diesel, there are vast interest in converting existing diesel light-duty trucks into those using CNG. To use CNG with compressed ignition (CI) engine, unless major engine modification is done, diesel is still needed in a smaller amount to initiate the combustion. CNG can be used as primary fuel and can be injected at intake ports. The so-called diesel-dual-fuel (DDF) engine concept can reduce total fuel cost while still obtain good performance of the CI engine.

The challenge comes from having two fuels in use at the same time. CNG is injected at the intake ports, which is mixed with fresh air before going into the combustion chamber. This spark-ignition (SI) engine-like behavior requires precise air path control. Diesel is also injected directly into the combustion chamber, where exhausted gas recirculation (EGR) amount must be carefully controlled. The more stringent performance requirement of the air path requires a high-performance control system.

Majority of the existing literature in air-path control is on the SI engine. In SI engine, the fuel injection is used to regulate the air/fuel ratio at a desired value. Some of the more recent works are as follows. Ref. [1] used the

second-order sliding mode control (SMC) with appropriately sliding gain to control the fueling amount to maintain a desired air/fuel ratio. Ref. [2] developed adaptive sliding gains to compensate the effect of time delay of oxygen sensor. Ref. [3] presented the adaptation of fuel-delivery model parameters and the measurement bias of air mass flow to deal with the problem caused by engine uncertainties. Some work includes designing an observer to estimate actual air inside the cylinder. Ref. [4] added the radial basis function neural network to replace observers for uncertainties compensation. Ref. [5] used observer-based SMC in which some states were estimated to reduce the plant model mismatch so that the chattering could be reduced. Ref. [6] presented a follow-up work with a direct adaptive control method using Gaussian neural networks to compensate transient fueling dynamics and the measurement bias of mass into the manifold.

Rather than controlling the fuel injection amount as in SI engine, EGR valve and variable geometry turbine (VGT) are normally used to control mass air flow (MAF) and manifold absolute pressure (MAP) in the air path of the CI engine. Several control strategies have been developed for controlling the air path of CI engine. Most control systems were designed from plant models such as transfer functions matrix as in Ref. [7]-[13] or linear or nonlinear state-space model as in Ref. [14]-[18]. Some control systems were designed without having the plant models in their algorithms. Ref. [19] used fuzzy logic control. Ref. [20] used the SMC for VGT control only. Ref. [21] developed the algorithm based on adaptive sliding mode control.

Since the DDF engine has CNG injected at intake ports and diesel fuel injected at the cylinders, its air-path control can mimic those of SI engine or CI engine. Like an SI engine, air/fuel ratio is controlled. However, the optimal desired air/fuel ratio is not fixed at one, but rather changes with operating points. Ref. [22] presented an algorithm in choosing to actuate either throttle or EGR valve to regulate air/fuel ratio of a DDF engine, while pumping loss is minimized. Ref. [23] is a follow-up work by adding the effect on adjusting the total fuel amount. Like a CI engine, MAF and MAP are controlled. Ref. [24] applied quantitative feedback theory (QFT) to control MAF and MAP from throttle and EGR valve.

In this paper, two multivariable SMC techniques were implemented and compared. The techniques have already existed in the literature but have not been used in air-path control applications. The SMC technique aim is to drive the system state variables to the origin. There are two phases: reaching and sliding. During reaching phase, the state variables are driven to a sliding surface and maintained there. During sliding phase, the state variables on the sliding surface moves to the origin. For tracking, a state-space model is formulated to have the tracking errors as its state variables. With SMC, the tracking errors are driven to the origin (zeros.) Some advantages over other techniques are as follows:

- Plant model is normally not required in the algorithm. However, knowing the plant model helps improving the quality of the control system in two ways. First, the plant model's upper bound can be used to compute, rather than trial-and-error, a controller parameter. Second, it can be feed-forwarded to cancel known terms. Doing so reduces the effort from fast-switching control, therefore reduces chattering.
- During sliding phase, the system order reduces from n to $n-m$, where n is the number of state variables and m is the number of control inputs. Reduced order consumes less computational time.
- During sliding phase, the system is not affected by matched uncertainties. Matched uncertainties are disturbances, noise, and plant uncertainties that can be directly altered by the control inputs.

Two SMC techniques used in this paper are model-reference SMC and integrator-augmented SMC. In model-reference SMC, a reference model, relating the reference to the plant output, is formulated to meet various time-domain specifications. Then, the SMC controller is designed so that the errors between the reference model state variables and the plant state variables are driven to zeros. As a result, the plant output is close to the reference model output, and the specifications can be met. In integrator-augmented SMC, a state variable,

representing integral of the tracking error, is augmented to the plant state variables. Then, the SMC controller is designed to drive all state variables to zeros.

The SMC used in this paper was based on the unit-vector approach, proposed in Ref. [25]. The unit-vector approach was shown to handle unmatched uncertainties effectively. The model-reference SMC and integrator-augmented SMC methods, suitable for tracking of multi-input-multi-output (MIMO) systems, were taken from Ref. [26]. Basics of the SMC method can be found from Ref. [26]- Ref. [28] and references therein. Stability analysis of nonlinear systems used in this paper can be found from Ref. [29].

A 2KD-FTV Toyota CI engine was modified as a DDF engine and was installed in a test cell with an engine dynamometer. CNG was injected at each intake port as in multi-point injection. Diesel was directly injected into each cylinder as liquid spark plug. Throttle and EGR valve were actuated to regulate MAF and MAP at various set points. Simulation and experimental results have shown that the MAF and MAP can follow their set points closely with benefits from the advantages of the SMC techniques mentioned above.

The paper presents topics in the following order:

- Air-path system identification
- Model-reference SMC design
- Integrator-augmented SMC design
- Experimental results
- Conclusions
- References, contact information, and acknowledgments

AIR-PATH SYSTEM IDENTIFICATION

A Toyota 2KD-FTV diesel engine was converted to a DDF engine and was installed in a test bed with an engine dynamometer. The test bed management system is AVL PUMA, and data acquisition and control hardware is National Instruments. Table 1 lists some important specifications of the engine.

Figure 1 depicts the air-path system of the engine. Parameters in Figure 1 describe measurable quantities from the engine test bed. $T,\ p, W, m$ are for temperature, pressure, mass flow rate, and mass, respectively. Subscripts $a, c,\ p, i, x, t, e$ are for ambient, compressor, plenum, intake manifold, exhausted manifold, turbine, and exhausted pipe, respectively. Throttle and EGR valves are two actuators to control MAF and MAP, which are denoted by W_{ac} and p_i in Figure 1.

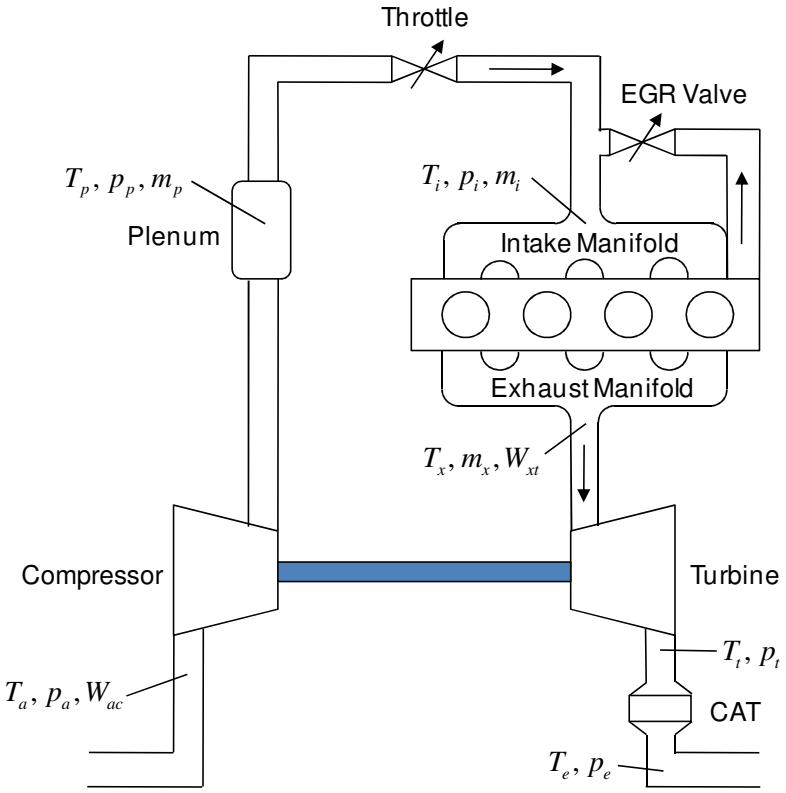

Figure 1: Air-path system of the DDF engine with measured signals.

Table 1: Engine Specifications

Model:	Toyota 2KD-FTV, Diesel Engine
Number of cylinders:	4 (Inline)
Number of valves:	16 (DOHC)
Manifold:	Cross-flow with turbocharger
Fuel system:	Common-rail direct injection
Displacement:	2,494 cc
Bore:	92.0 mm
Stroke:	93.8 mm
Connecting rod:	158.5 mm
Compression ratio:	18.5:1
Max power:	75 kW at 3,600 rpm
Max torque:	260 Nm at 1,600 - 2,400 rpm
Valve timings:	
IVO	718 deg CA
IVC	211 deg CA
EVO	510 deg CA
EVC	0 deg CA
Firing order:	1-3-4-2

To find a plant model relating throttle duty cycle (%) and EGR valve duty cycle (%) to MAF (kg/hr) and MAP (kPa), three facts are used:

- Fixed maps, obtained during engine calibration, provide required values of nominal throttle position (TPS) and EGR to obtain specific values of MAF and MAP. These nominal values of TPS and EGR are used as feed-forward term in control system. Since the controller only handles deviations from the fixed maps, the plant transfer function matrix only relates the deviations of inputs to the deviations of outputs. Therefore, in finding the plant transfer function matrix, mean values of all signals are removed.
- EGR moves in the opposite direction to MAP and MAF, that is, increasing EGR results in decreasing MAP and MAF and vice versa. Therefore, transfer functions relating ΔEGR to ΔMAP and ΔMAF have non-minimum-phase zeros, which limit controller performance. Transfer functions from $-\Delta EGR$ to ΔMAP and ΔMAF are used instead to avoid the non-minimum-phase problem.
- The engine runs with medium speed (2000 rpm) and load (20% pedal.)

The two-by-two plant transfer function matrix is found as

$$\begin{bmatrix} \Delta MAF \\ \Delta MAP \end{bmatrix} = \begin{bmatrix} p_{11} & p_{12} \\ p_{21} & p_{22} \end{bmatrix} \begin{bmatrix} \Delta THRdc \\ -\Delta EGRdc \end{bmatrix} = \begin{bmatrix} \dfrac{0.167}{0.049s+1} & \dfrac{1.128}{0.132s+1} \\ \dfrac{0.221(0.033s+1)}{0.1621s+1} & \dfrac{0.116}{0.419s+1} \end{bmatrix} \begin{bmatrix} \Delta THRdc \\ -\Delta EGRdc \end{bmatrix}, \tag{1}$$

where $\Delta THRdc$ represents the deviation of the throttle duty cycle from its mean value, $\Delta EGRdc$ represents the deviation of the EGR valve duty cycle form its mean value, ΔMAF represents the deviation of the mass air flow (kg/hr) from its mean value, ΔMAP represents the deviation of the manifold absolute pressure (kPa) from its mean value. s represents the complex variable in the transfer function.

p_{11} and p_{21} are found by closing the EGR valve fully and inputting a frequency-varying square wave as $\Delta THRdc$. p_{12} and p_{22} are found by opening TPS fully and inputting a frequency-varying square wave as $\Delta EGRdc$. After removing means from all signals, a Matlab function, *ident*, is used to find the transfer functions.

A state-space plant model in regular form, obtained from (1) with Matlab functions *ss*, *ssdata*, and *ctrbf*, is given by

$$\begin{bmatrix} \dot{x}_1 \\ \dot{x}_2 \\ \dot{x}_3 \\ \dot{x}_4 \end{bmatrix} = \left[\begin{array}{c|c} A_{11} & A_{12} \\ \hline A_{21} & A_{22} \end{array}\right] \begin{bmatrix} x_1 \\ x_2 \\ x_3 \\ x_4 \end{bmatrix} + \begin{bmatrix} B_1 \\ \hline B_2 \end{bmatrix} \begin{bmatrix} u_1 \\ u_2 \end{bmatrix},$$

$$= \left[\begin{array}{cc|cc} -2.568 & -0.809 & 0.713 & -0.630 \\ -0.809 & -8.945 & 5.710 & 0.078 \\ \hline 0.713 & 5.710 & -17.680 & 0 \\ -0.630 & 0.078 & 0 & -7.467 \end{array}\right] \begin{bmatrix} x_1 \\ x_2 \\ x_3 \\ x_4 \end{bmatrix} + \left[\begin{array}{cc} 0 & 0 \\ 0 & 0 \\ \hline -2.236 & 0 \\ 0 & -4.031 \end{array}\right] \begin{bmatrix} u_1 \\ u_2 \end{bmatrix}, \tag{2}$$

$$\begin{bmatrix} y_1 \\ y_2 \end{bmatrix} = \begin{bmatrix} C_1 & C_2 \end{bmatrix} \begin{bmatrix} x_1 \\ x_2 \\ x_3 \\ x_4 \end{bmatrix} = \left[\begin{array}{cc|cc} -0.166 & 0.792 & -1.532 & -2.111 \\ 0.425 & -1.029 & -0.484 & -0.068 \end{array}\right] \begin{bmatrix} x_1 \\ x_2 \\ x_3 \\ x_4 \end{bmatrix},$$

where u_1 is $\Delta THRdc$, u_2 is $-\Delta EGRdc$, y_1 is ΔMAF, y_2 is ΔMAP, and $x = \begin{bmatrix} x_1, x_2, x_3, x_4 \end{bmatrix}^T$ is a vector containing state variables.

The model is validated using different set of data, obtained from letting both $\Delta THRdc$ and $\Delta EGRdc$ be frequency-varying square waves simultaneously. As shown in Figure 2, the frequencies of the model outputs match those of the actual outputs closely. However, the amplitudes do not match quite well, especially those of the ΔMAF model. This mismatch will be handled by the proposed SMC techniques.

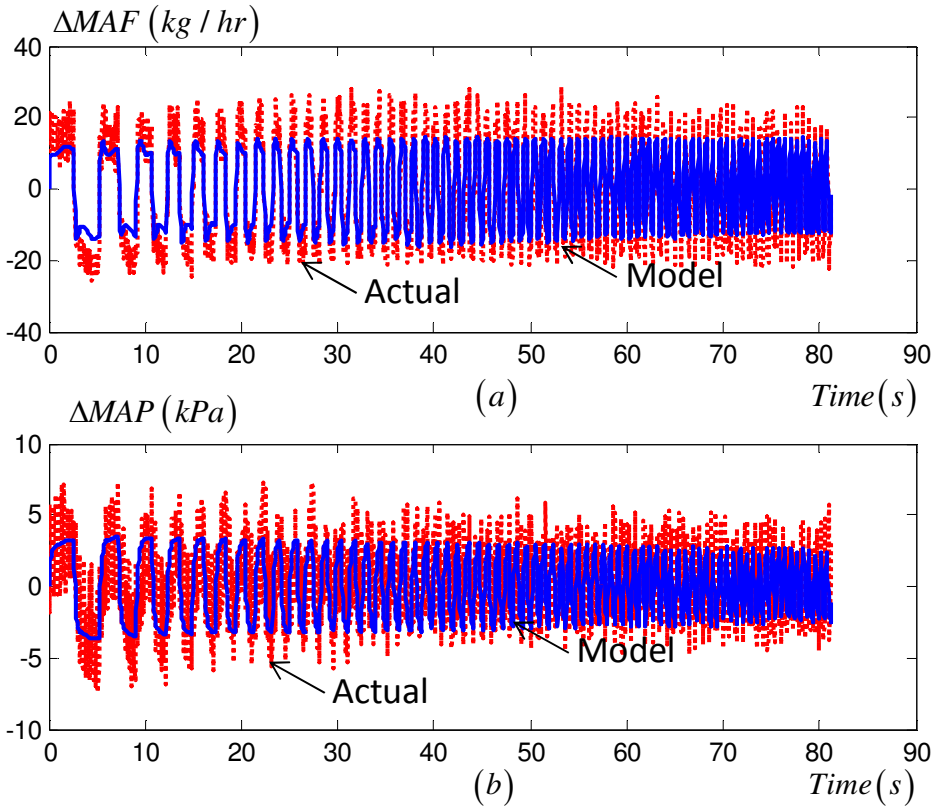

Figure 2: Model validation using a different set of data. Dash lines are actual values. Solid lines are model values. (a) $\Delta MAF\left(kg / hr\right)$. (b) $\Delta MAP\left(kPa\right)$.

MODEL-REFERENCE SMC DESIGN

PLANT MODEL

Consider a plant model

$$\begin{aligned} \dot{x} &= Ax + Bu, \\ y &= Cx, \end{aligned} \tag{3}$$

where $x \in \mathbb{R}^n$ is a vector of state variables, $y \in \mathbb{R}^m$ is a vector of plant outputs, $u \in \mathbb{R}^m$ is a vector of control inputs. A, B, and C are constant matrices with corresponding dimensions.

If $rank\left(B\right) = m$ and the pair $\left(A, B\right)$ is controllable, the plant model can be transformed into regular form as

$$\begin{aligned} \begin{bmatrix} \dot{x}_1 \\ \dot{x}_2 \end{bmatrix} &= \left[\begin{array}{c|c} A_{11} & A_{12} \\ \hline A_{21} & A_{22} \end{array}\right] \begin{bmatrix} x_1 \\ x_2 \end{bmatrix} + \begin{bmatrix} 0 \\ \hline B_2 \end{bmatrix} u, \\ y &= \left[\begin{array}{c|c} C_1 & C_2 \end{array}\right] \begin{bmatrix} x_1 \\ x_2 \end{bmatrix}, \end{aligned} \tag{4}$$

where $x_1 \in \mathbb{R}^{n-m}$, $x_2 \in \mathbb{R}^m$, $A_{11}, A_{12}, A_{21}, A_{22}, B_2, C_1,$ and C_2 are constant matrices with corresponding dimensions.

REFERENCE MODEL

Consider another reference model

$$\begin{aligned} \dot{w} &= A_m w + B_m r, \\ y_m &= Cw, \end{aligned} \tag{5}$$

where $w \in \mathbb{R}^n$ is a vector of state variables, $y_m \in \mathbb{R}^m$ is a vector of reference model outputs, $r \in \mathbb{R}^m$ is a vector of reference inputs. $A_m, B_m,$ and C are constant matrices with corresponding dimensions.

If $rank\left(B_m\right) = m$ and the pair $\left(A_m, B_m\right)$ is controllable, the reference model can be transformed into regular form as

$$\left[\begin{array}{c} \dot{w}_1 \\ \hline \dot{w}_2 \end{array}\right] = \left[\begin{array}{c|c} A_{m11} & A_{m12} \\ \hline A_{m21} & A_{m22} \end{array}\right]\left[\begin{array}{c} w_1 \\ \hline w_2 \end{array}\right] + \left[\begin{array}{c} 0 \\ \hline B_{m2} \end{array}\right] r,$$

$$y_m = \left[C_1 \mid C_2\right]\left[\begin{array}{c} w_1 \\ \hline w_2 \end{array}\right],$$

where $w_1 \in \mathbb{R}^{n-m}$, $w_2 \in \mathbb{R}^m$, $A_{m11}, A_{m12}, A_{m21}, A_{m22}, B_{m2}, C_1,$ and C_2 are constant matrices with corresponding dimensions.

The reference model $\left(A_m, B_m\right)$ can be formulated so that the model outputs follow the reference inputs with desirable transient response. The control inputs u can then be designed to make x track w so that y tracks y_m.

One way to find the matrices A_m and B_m is to use pole-placement method. Suppose we want to design u for the plant model (3) to have desirable closed-loop poles and to ensure steady-state tracking of a step reference, we choose

$$u = Fx + Gr.$$

The closed-loop system becomes $\dot{x} = \left(A + BF\right)x + BGr$, $y = Cx$ and the transfer function from r to y is given by

$$\frac{y(s)}{r(s)} = C\left(sI - \left(A + BF\right)\right)^{-1} BG.$$

A full-state feedback matrix F can be designed to place the closed-loop poles at desired locations to achieve desirable transient response. To ensure steady-state tracking of a step reference, using the final-value theorem,

$$G = -\left(C\left(A+BF\right)^{-1}B\right)^{-1}.$$

Therefore, the reference model can be chosen as $A_m = A + BF$ and $B_m = BG$.

CONTROL LAW

The control inputs u will be designed to make x track w so that y tracks y_m. Let $e = x - w$ be the error between the plant state variables and the reference model state variables. From (3) and (5), the error dynamics are given by

$$\dot{e} = A_m e + \left(A - A_m\right)x + Bu - B_m r. \tag{6}$$

Consider a control law

$$u = u_l + u_n + u_2 = v + u_2, \tag{7}$$

where

$$u_2 = B^{\dagger}\left(A_m - A\right)x + B^{\dagger}B_m r \tag{8}$$

is an inverse dynamics term with $B^{\dagger}$ as pseudo-inverse of B and u_l and u_n are to be designed.

Substituting (7) into (6), we have $\dot{e} = A_m e + Bv$. Since both plant model and reference model are in regular form, the error dynamics can also be written in regular form as

$$\begin{aligned}\dot{e}_1 &= A_{m11}e_1 + A_{m12}e_2,\\ \dot{e}_2 &= A_{m21}e_1 + A_{m22}e_2 + B_2 v.\end{aligned} \tag{9}$$

Let the switching surface be

$$s = Se = S_1 e_1 + S_2 e_2 = S_2 M e_1 + S_2 e_2, \tag{10}$$

where S, S_1, S_2, and M are constant matrices with appropriate dimensions.

Choose $S_2 B_2 = \Lambda,$ where Λ is any nonsingular diagonal matrix, normally chosen to be B_2 so that $S_2 = I$.

Using a linear change of coordinates

$$T_s \triangleq \begin{bmatrix} I & 0 \\ S_1 & S_2 \end{bmatrix},$$

we have

$$\begin{bmatrix} e_1 \\ s \end{bmatrix} = T_s \begin{bmatrix} e_1 \\ e_2 \end{bmatrix}. \tag{11}$$

Choose

$$u_l = -\left(SB\right)^{-1}\left(SA_m - \Phi S\right)e, \tag{12}$$

where Φ is any stable design matrix,

and choose

$$u_n = -\rho\left(SB\right)^{-1}\frac{P_2 s}{\left\|P_2 s\right\|}, \tag{13}$$

where $\rho > 0$ is a design parameter and P_2 is a symmetric positive definite matrix satisfying the Lyapunov equation

$$P_2\Phi + \Phi^T P_2 = -I. \tag{14}$$

Using (11)-(13) with (9) and after a straight-forward derivation, we have

$$\dot{e}_1 = \left(A_{m11} - A_{m12}M\right)e_1 + \left(A_{m12}S_2^{-1}\right)s, \tag{15}$$

$$\dot{s} = \Phi s - \rho\frac{P_2 s}{\left\|P_2 s\right\|}.$$

Consider a Lyapunov function $V_1 = s^T P_2 s > 0,$ whose derivative is given by

$$\begin{aligned} \dot{V}_1 &= \dot{s}^T P_2 s + s^T P_2 \dot{s} \\ &\le -\left\|s\right\|^2 - 2\rho\left\|P_2 s\right\| \\ &\le -2\rho\sqrt{\lambda_{\min}\left(P_2\right)}\sqrt{V_1} \\ &< 0. \end{aligned} \tag{16}$$

The derivation above uses the fact that $s^T P_2 P_2 s = \left\|P_2 s\right\|^2$ and the Rayleigh principle

$$\left\|P_2 s\right\|^2 = \left(P_2^{1/2}s\right)^T P_2\left(P_2^{1/2}s\right) \ge \lambda_{\min}\left(P_2\right)\left\|P_2^{1/2}s\right\|^2 = \lambda_{\min}\left(P_2\right)V_1,$$

where $\lambda_{\min}\left(P_2\right)$ is minimum eigenvalue of P_2.

From (16), we can conclude that s will approach zeros in finite time and will remain there afterward.

Consider another Lyapunov function $V_2 = e_1^T P_1 e_1 > 0,$ where P_1 is a unique symmetric positive definite solution to the Lyapunov equation $P_1\left(A_{m11} - A_{m12}M\right) + \left(A_{m11} - A_{m12}M\right)^T P_1 = -Q_1,$ where Q_1 is a design symmetric positive definite matrix and M is designed so that $\left(A_{m11} - A_{m12}M\right)$ is a stable matrix. Substituting $s = 0$ into (15), $\dot{V}_2$ can be computed as

$$\begin{aligned}\dot{V}_2 &= \dot{e}_1^T P_1 e_1 + e_1^T P_1 \dot{e}_1 \\ &= -e_1^T Q_1 e_1 \\ &< 0.\end{aligned} \tag{17}$$

From (17), we can conclude that e_1 will approach zeros in finite time and will remain there afterward. From (10), with $s = 0,$ e_2 will also approach zeros.

CONTROL DESIGN

In our case, the plant model in regular form (4) is given by (2). The reference model (5) is found, by placing the poles of (A, B) at -3, -3, -6, and -6 using Matlab command *place*, as

$$\begin{bmatrix}\dot{w}_1 \\ \dot{w}_2 \\ \dot{w}_3 \\ \dot{w}_4\end{bmatrix} = \left[\begin{array}{c|c} A_{m11} & A_{m12} \\ \hline A_{m21} & A_{m22}\end{array}\right]\begin{bmatrix}w_1 \\ w_2 \\ w_3 \\ w_4\end{bmatrix} + \left[\begin{array}{c} 0 \\ \hline B_{m2}\end{array}\right]\begin{bmatrix}r_1 \\ r_2\end{bmatrix},$$

$$= \left[\begin{array}{cc|cc} -2.568 & -0.809 & 0.713 & -0.630 \\ -0.809 & -8.945 & 5.710 & 0.078 \\ \hline -0.397 & -3.176 & 0.046 & 0 \\ 2.944 & -0.368 & 0 & -6.533\end{array}\right]\begin{bmatrix}w_1 \\ w_2 \\ w_3 \\ w_4\end{bmatrix} + \left[\begin{array}{cc} 0 & 0 \\ 0 & 0 \\ \hline 0.206 & -2.005 \\ -3.957 & 3.758\end{array}\right]\begin{bmatrix}r_1 \\ r_2\end{bmatrix},$$

$$\begin{bmatrix}y_{m1} \\ y_{m2}\end{bmatrix} = \left[C_1 \mid C_2\right]\begin{bmatrix}w_1 \\ w_2 \\ w_3 \\ w_4\end{bmatrix} = \left[\begin{array}{cc|cc} -0.166 & 0.792 & -1.532 & -2.111 \\ 0.425 & -1.029 & -0.484 & -0.068\end{array}\right]\begin{bmatrix}w_1 \\ w_2 \\ w_3 \\ w_4\end{bmatrix}.$$

Choose M by placing the poles of $\left(A_{m11}, A_{m12}\right)$ at -50 and -100 as

$$M = \begin{bmatrix} 0.882 & 15.684 \\ -74.279 & 19.051\end{bmatrix}.$$

Choose $\Lambda = B_2$ so $S_2 = I.$ The switching surface is then given by $s = Se = S_1 e_1 + S_2 e_2 = Me_1 + e_2,$ where $S = \left[M \mid I\right].$

Choose $P_2 = I.$ Φ is then found from (14) using Matlab command *lyap* as

$$\Phi = \begin{bmatrix} -0.5 & 0 \\ 0 & -0.5 \end{bmatrix}.$$

Choose $\rho = 1$. The control law is given by (7), (8), (12), and (13).

INTEGRATOR-AUGMENTED SMC DESIGN

CONTROL LAW

Consider again the plant model (3)

$$\dot{x} = Ax + Bu,$$
$$y = Cx.$$

Introduce integral-action state variables $x_r \in \mathbb{R}^m$, satisfying

$$\dot{x}_r = r - y,$$

where the reference inputs r satisfies

$$\dot{r} = \Gamma(r - R),$$

where Γ is a stable design matrix and R is a constant demand vector.

The plant model state variables, augmented by the integral-action state variables, are given by

$\tilde{x} = \begin{bmatrix} x_r \\ x \end{bmatrix}$, where $x_r \in \mathbb{R}^m$ and $x \in \mathbb{R}^n$. which can be re-partitioned as $\tilde{x} = \begin{bmatrix} x_1 \\ x_2 \end{bmatrix}$, where $x_1 \in \mathbb{R}^n$ and $x_2 \in \mathbb{R}^m$.

The augmented system then becomes

$$\begin{aligned} \dot{x}_1 &= \tilde{A}_{11}x_1 + \tilde{A}_{12}x_2 + B_r r, \\ \dot{x}_2 &= \tilde{A}_{21}x_1 + A_{22}x_2 + B_2 u, \end{aligned} \tag{18}$$

where

$$\begin{bmatrix} \tilde{A}_{11} & \tilde{A}_{12} \\ \tilde{A}_{21} & A_{22} \end{bmatrix} \triangleq \left[\begin{array}{cc:c} 0 & -C_1 & -C_2 \\ 0 & A_{11} & A_{12} \\ \hdashline 0 & A_{21} & A_{22} \end{array}\right] \text{ and } B_r = \begin{bmatrix} I_m \\ 0 \end{bmatrix}.$$

Let the switching surface be

$$\overline{s} = S\tilde{x} - S_r r = S_1 x_1 + S_2 x_2 - S_r r = S_2 M x_1 + S_2 x_2 - S_r r, \tag{19}$$

where $S, S_1, S_2, S_r,$ and M are constant matrices with appropriate dimensions.

Choose $S_2 B_2 = \Lambda,$ where Λ is any nonsingular diagonal matrix.

Choose the control inputs

$$u = u_l + u_n \tag{20}$$

with

$$u_l = -\left(S_2 B_2\right)^{-1}\left(S\begin{bmatrix} \tilde{A}_{11} & \tilde{A}_{12} \\ \tilde{A}_{21} & A_{22} \end{bmatrix} - \Phi S \right)\tilde{x} - \left(S_2 B_2\right)^{-1}\left(\Phi S_r + S_1 B_r\right) r + \left(S_2 B_2\right)^{-1} S_r \dot{r}, \tag{21}$$

where Φ is any stable design matrix,

and choose

$$u_n = -\rho\left(SB\right)^{-1}\frac{P_2\left(\overline{s}\right)}{\left\|P_2\left(\overline{s}\right)\right\|}, \tag{22}$$

where $\rho > 0$ is a design parameter and P_2 is a symmetric positive definite matrix satisfying the Lyapunov equation

$$P_2\Phi + \Phi^T P_2 = -I. \tag{23}$$

Using (19)-(22) with (18) and after a straight-forward derivation, we have

$$\dot{x}_1 = \left(\tilde{A}_{11} - \tilde{A}_{12}M\right)x_1 + \tilde{A}_{12}S_2^{-1}\overline{s} + \left(\tilde{A}_{12}S_2^{-1}S_r + B_r\right)r, \tag{24}$$

$$\dot{\overline{s}} = \Phi\overline{s} - \rho\frac{P_2\overline{s}}{\left\|P_2\overline{s}\right\|}.$$

Consider a Lyapunov function $V_1 = \overline{s}^T P_2 \overline{s} > 0,$ whose derivative is given by

$$\begin{aligned} \dot{V}_1 &= \dot{\overline{s}}^T P_2\overline{s} + \overline{s}^T P_2\dot{\overline{s}} \\ &\le -\left\|\overline{s}\right\|^2 - 2\rho\left\|P_2\overline{s}\right\| \\ &\le -2\rho\sqrt{\lambda_{\min}\left(P_2\right)}\sqrt{V_1} \\ &< 0. \end{aligned} \tag{25}$$

The derivation above uses the fact that $\overline{s}^T P_2 P_2 \overline{s} = \left\|P_2\overline{s}\right\|^2$ and the Rayleigh principle

$$\left\|P_2\overline{s}\right\|^2 = \left(P_2^{1/2}\overline{s}\right)^T P_2\left(P_2^{1/2}\overline{s}\right) \ge \lambda_{\min}\left(P_2\right)\left\|P_2^{1/2}\overline{s}\right\|^2 = \lambda_{\min}\left(P_2\right)V_1,$$

where $\lambda_{\min}(P_2)$ is minimum eigenvalue of P_2.

From (25), we can conclude that $\bar{s}$ will approach zeros in finite time and will remain there afterward.

Consider another Lyapunov function $V_2 = x_1^T P_1 x_1 > 0,$ where P_1 is a unique symmetric positive definite solution to the Lyapunov equation $P_1\left(\tilde{A}_{11} - \tilde{A}_{12}M\right) + \left(\tilde{A}_{11} - \tilde{A}_{12}M\right)^T P_1 = -Q_1,$ where Q_1 is a design symmetric positive definite matrix and M is designed so that $\left(\tilde{A}_{11} - \tilde{A}_{12}M\right)$ is a stable matrix. Substituting $\bar{s} = 0$ into (24), $\dot{V}_2$ can be computed as

$$\begin{aligned}\dot{V}_2 &= \dot{x}_1^T P_1 x_1 + x_1^T P_1 \dot{x}_1 \\ &= -x_1^T Q_1 x_1 + 2x_1^T P_1\left[\left(\tilde{A}_{12}S_2^{-1}S_r + B_r\right)r\right] \\ &\le -\lambda_{\min}(Q_1)\|x_1\|^2 + 2\|x_1\|\lambda_{\max}(P_1)b \\ &= -\|x_1\|\lambda_{\max}(P_1)\left[\frac{\lambda_{\min}(Q_1)}{\lambda_{\max}(P_1)}\|x_1\| - 2b\right],\end{aligned}$$

where $\left\|\left(\tilde{A}_{12}S_2^{-1}S_r + B_r\right)r\right\| \le b.$

If $b < \frac{1}{2}\frac{\lambda_{\min}(Q_1)}{\lambda_{\max}(P_1)}\|x_1\|,$ we have

$$\dot{V}_2 < 0. \tag{26}$$

From (26), we can conclude that x_1 will approach zeros in finite time and will remain there afterward. Therefore, $x_r,$ which is integral of tracking error, will also approach zeros.

CONTROL DESIGN

Consider the plant model in regular form (2). For the reference inputs, choose $\Gamma = \begin{bmatrix} -2 & 0 \\ 0 & -2 \end{bmatrix}$ and $R = \begin{bmatrix} 0.1 \\ 0.1 \end{bmatrix}$.

Choose $\Lambda = \begin{bmatrix} 1000 & 0 \\ 0 & 1000 \end{bmatrix}$. Choose M to place the poles of $\left(\tilde{A}_{11}, \tilde{A}_{12}\right)$ at -1, -1, -2, and -2 as

$M = \begin{bmatrix} -0.0229 & 0.2227 & -0.1835 & -1.0487 \\ 0.4397 & -0.4176 & 0.5625 & -0.1529 \end{bmatrix}$. The sliding surface matrices are given by

$$S_1 = \begin{bmatrix} 10.2399 & -99.6084 & 82.0827 & 468.9968 \\ -109.0783 & 103.5848 & -139.5350 & 37.9223 \end{bmatrix},$$

$S_2 = \begin{bmatrix} -447.2136 & 0 \\ 0 & -248.0695 \end{bmatrix}$, and $S_r = \begin{bmatrix} 1 & 0 \\ 0 & 1 \end{bmatrix}$.

Choose $P_2 = \begin{bmatrix} 1 & 0 \\ 0 & 1 \end{bmatrix}$ to obtain $\Phi = \begin{bmatrix} -0.5 & 0 \\ 0 & -0.5 \end{bmatrix}$. Choose $\rho = 1$.

The control law is given by (20) whose components are given by (21) and (22).

EXPERIMENTAL RESULTS

The model reference SMC and integrator-augmented SMC were implemented with an engine test bed. A 2KD-FTV Toyota engine was modified to a DDF engine by injecting CNG at each intake ports. The engine was connected to an eddy-current type engine dynamometer. The dynamometer management system was AVL PUMA and the control algorithm was written in Labview running National Instruments' hardware with 50 milliseconds for the sampling rate of data acquisition. All experiments were performed at medium load (20% pedal position) and medium speed (2000 rpm.)

Figure 3 contains a block diagram of the closed-loop system implementation. Two maps determined desired MAP and MAF from engine speed and load. These desired MAP and MAF values were passed to other two maps to determine nominal throttle and EGR valve duty cycles. These values were used as feed-forward terms.

The sliding-mode controllers generated Δ throttle duty cycle and $-\Delta$ EGR valve duty cycle. After the minus sign conversion, they were added to the feed-forward terms to become throttle and EGR valve duty cycles. These duty cycles belonged to pulse width modulation (PWM) signals used to actuate the throttle and EGR valve.

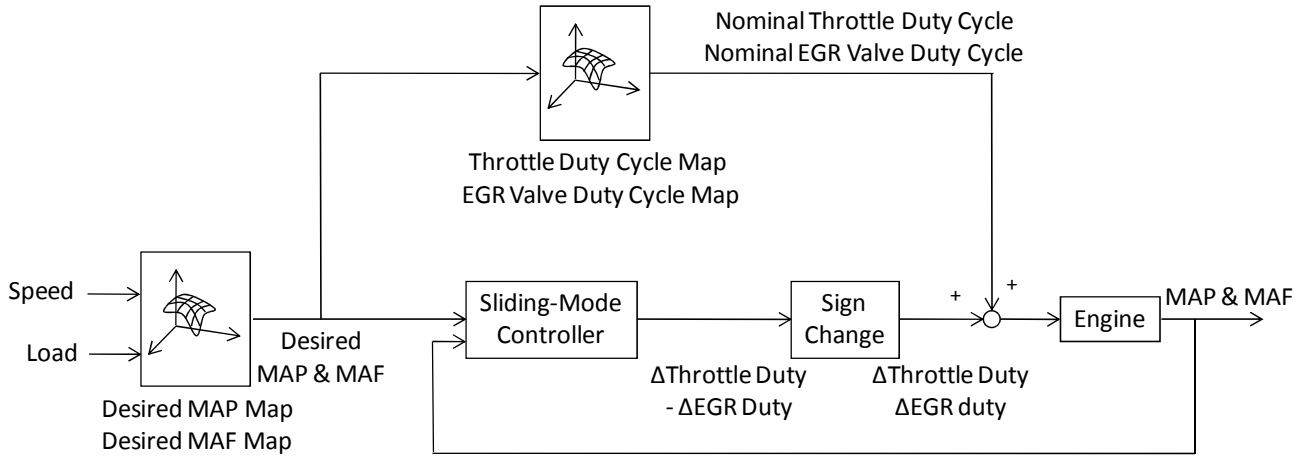

Figure 3: Implemented closed-loop system.

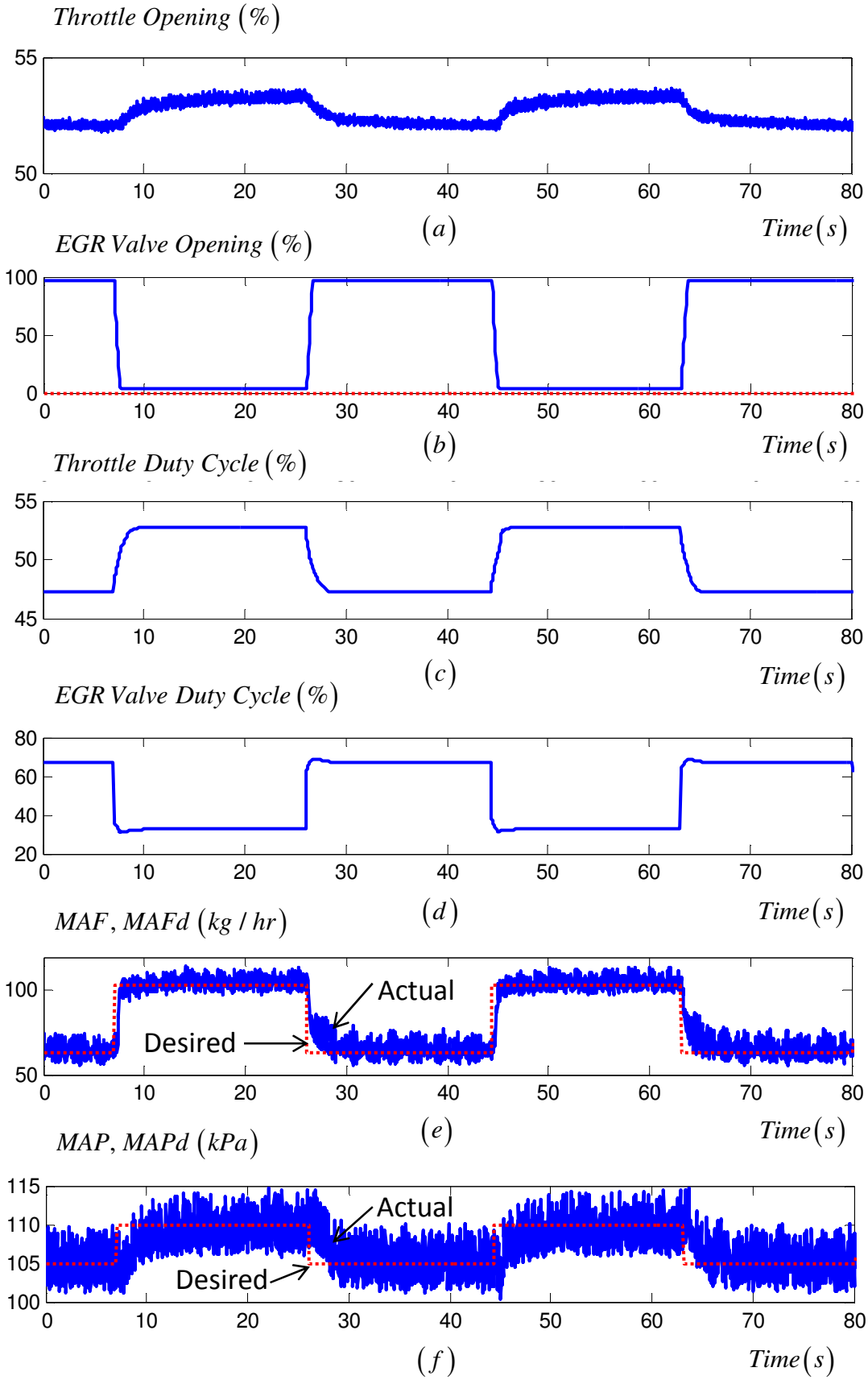
Throttle Opening (%)
55
50
0 10 20 30 40 50 60 70 80
(a)
Time(s)
EGR Valve Opening (%)
100
50
0
0 10 20 30 40 50 60 70 80
(b)
Time(s)
Throttle Duty Cycle (%)
55
50
45
0 10 20 30 40 50 60 70 80
(c)
Time(s)
EGR Valve Duty Cycle (%)
80
60
40
20
0 10 20 30 40 50 60 70 80
(d)
Time(s)
MAF, MAFd (kg / hr)
100
50
Actual
Desired
0 10 20 30 40 50 60 70 80
(e)
Time(s)
MAP, MAPd (kPa)
115
110
105
100
Actual
Desired
0 10 20 30 40 50 60 70 80
(f)
Time(s)

Figure 4: Experimental results from using the model-reference SMC. (a) Throttle opening (%). (b) EGR valve opening (%). (c) Throttle duty cycle (%). (d) EGR valve duty cycle (%). (e) MAF and its desired value MAFd in kg/hr. (f) MAP and its desired value MAPd in kPa.

Figure 4 shows the experimental results from using the model-reference SMC. The actual MAF and MAP were able to follow their desired values closely as can be seen from Figure 4(e) and (f). The qualities of the response, such as overshoot, settling time, and steady-state error, met our specifications (i.e., 10% overshoot, 3% (or 2.5 s) settling time, and ±10 steady-state error). Figure 4(c) and (d) contain throttle and EGR valve duty cycles, whereas Figure 4(a) and (b) are the corresponding throttle and EGR valve openings. The control chattering normally seen with SMC was not present in this case because of the inverse dynamics terms u_2, which represented most of the control efforts.

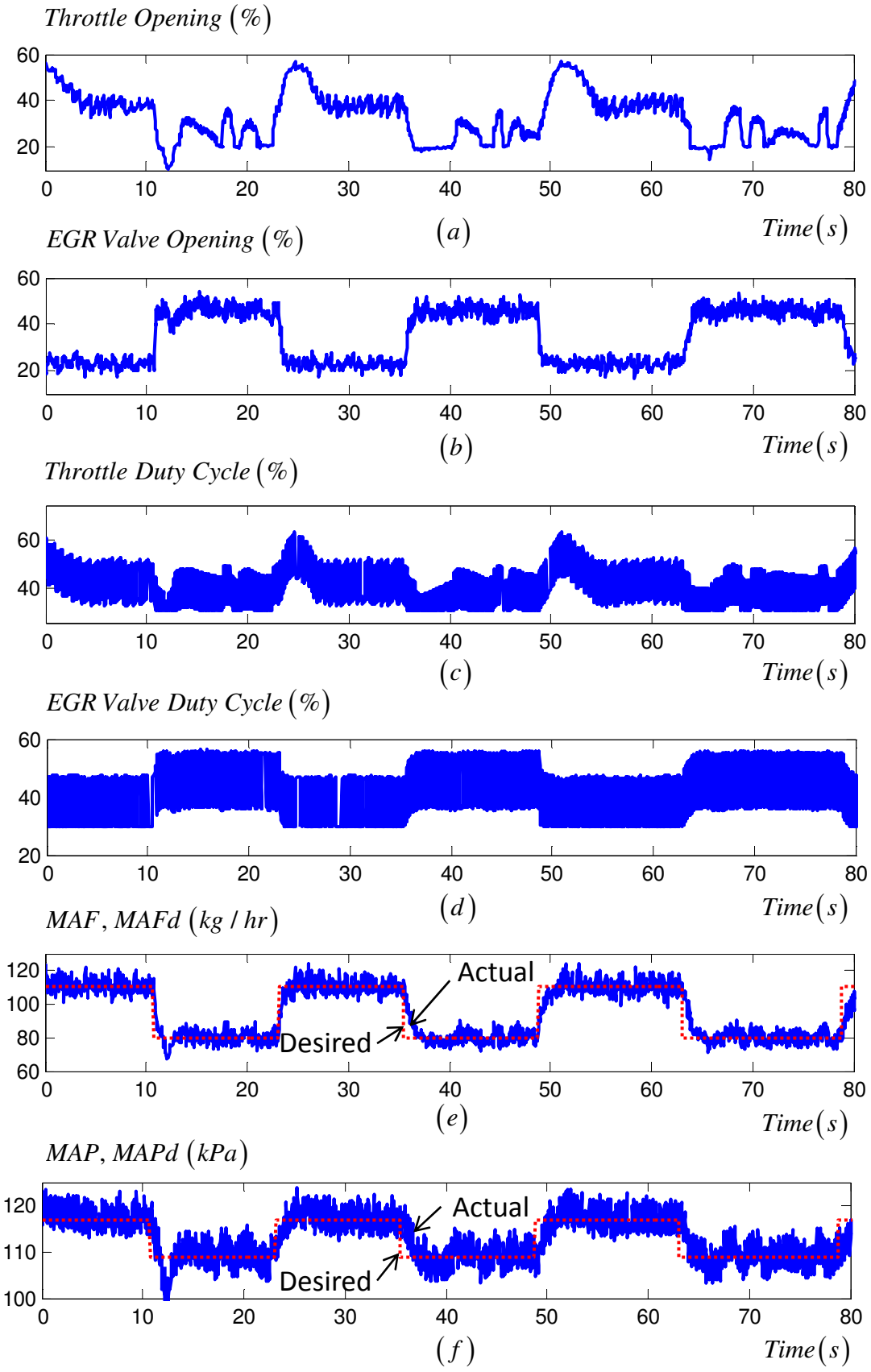
Throttle Opening (%)
60
40
20
0 10 20 30 40 50 60 70 80
(a)
Time(s)
EGR Valve Opening (%)
60
40
20
0 10 20 30 40 50 60 70 80
(b)
Time(s)
Throttle Duty Cycle (%)
60
40
0 10 20 30 40 50 60 70 80
(c)
Time(s)
EGR Valve Duty Cycle (%)
60
40
20
0 10 20 30 40 50 60 70 80
(d)
Time(s)
MAF, MAFd (kg / hr)
120
100
80
60
Actual
Desired
0 10 20 30 40 50 60 70 80
(e)
Time(s)
MAP, MAPd (kPa)
120
110
100
Actual
Desired
0 10 20 30 40 50 60 70 80
(f)
Time(s)

Figure 5: Experimental results from using the integrator-augmented SMC. (a) Throttle opening (%). (b) EGR valve opening (%). (c) Throttle duty cycle (%). (d) EGR valve duty cycle (%). (e) MAF and its desired value MAFd in kg/hr. (f) MAP and its desired value MAPd in kPa.

Figure 5 shows the experimental results from using the integrator-augmented SMC. The actual MAF and MAP were able to follow their desired values closely as can be seen from Figure 5(e) and (f). Figure 5(c) and (d) contain throttle and EGR valve duty cycles, whereas Figure 5(a) and (b) are the corresponding throttle and EGR valve openings. The control chattering was present because there was no inverse dynamics terms as in the model-reference SMC. The fast-switching control u_n contributed more of the total control efforts in this case. Various methods have been available to reduce control chattering. The readers can consult Ref. [26]-[28] for details.

In our experiences, the model-reference SMC has advantages and disadvantages over the integrator-augmented SMC as follows:

Advantages of the model-reference SMC

- The time-domain specifications such as rise time, settling time, overshoot, and steady-state error can be specified via using the method of pole-placement in the reference model.
- Less control chattering due to the inverse dynamics terms u_2, which contribute most of the control efforts.

Disadvantages of the model-reference SMC

- The reference model may contain model uncertainties if it is obtained from the uncertain plant model.
- The method has no feedback and relies on the accuracy of the plant and reference models. If the model uncertainties are too much, the fast-switching control might not be able to handle the uncertainties resulting in non-zero steady-state error.
- More efforts are required in finding accurate plant model and formulating the reference model.

CONCLUSIONS

Two multi-variable SMC techniques were implemented with MAF and MAP tracking of a DDF engine. Due to the mixed behaviors between the SI and CI engines of the DDF engine, its air path requires higher-performance controllers. Even though the SMC is well-known in applications, its multi-variable tracking problem is not trivial. In this paper, two SMC techniques, one follows reference model, the other uses integrator to obtain zero steady-state error, were studied and compared. The Experimental results (2000 rpm and 20% paddle) showed that the MAP and MAF responses from both techniques were able to track their desired values in 2.5 seconds settling time and less than 10% overshoot. The plant model (1) remains effective within the vicinity of that engine operation. However at some of the extreme operating points, such as the ones that only use diesel, a new plant model, for which the controller is to be designed, should be found. Other techniques, such as gain-scheduling or adaptive gain, can be used to switch among the controllers for different operating points. The chattering of those responses in the integrator-augmented SMC is more than the model-reference SMC since it has no inverse dynamics terms. However, both techniques have their own advantages and disadvantages and can both be used to control the engine air path effectively as can be seen from the experimental results.

In the future, more extensive experiments should be performed such as engine speed and load changes, arbitrary set point changes, new European driving cycle (NEDC) test, and road test with commercial truck. More

elaborated SMC techniques such as nonlinear sliding surface, SMC that uses nonlinear plant model, integral SMC that eliminates reaching phase, should be trialed.

SMC techniques can also be fused with other controller design techniques. Intelligent system such as fuzzy system may be used to supply the nominal duty cycles, which may change with operating points or time. Real-time system identification techniques such as recursive least squares and gradient methods can also be used to identify the plant model on-line.

REFERENCES

[1] Wang, S. and Yu, D. L., "An Application of Second-Order Sliding Mode Control for IC Engine Fuel Injection," *Proc. IEEE,* pp. 1035-1038, 2006.

[2] Wang, S. and Yu, D. L., "A New Development of Internal Combustion Engine Air-Fuel Ratio Control with Second-Order Sliding Mode," *ASME J. Dyn. Syst., Meas., Control* **129**:757-766, 2007.

[3] Yoon, P. and Sunwoo, M., "An Adaptive Sliding Mode Controller for Air-Fuel Ratio Control of Spark Ignition Engines," *Proc. Inst. Mech. Eng., Part D (J. Automob. Eng.)* **215**:305-315, 2001.

[4] Souder, J. S. and Hedrick, J. K., "Adaptive Sliding Mode Control of Air–Fuel Ratio in Internal Combustion Engines," *Int. J. Robust Nonlinear Control* **14**:525-541, 2004.

[5] Choi, S. B. and Hedrick, J. K., "An Observer-Based Controller Design Method for Improving Air/Fuel Characteristics of Spark Ignition Engines," *IEEE Trans. Control Syst. Technol.* **6**(3):325-334, 1998.

[6] Won, M., Choi, S. B., and Hedrick, J. K., "Air-to-Fuel Ratio Control of Spark Ignition Engines Using Gaussian Network Sliding Control," *IEEE Trans. Control Syst. Technol.* **6**(5):678-687, 1998.

[7] Alfieri, E., Amstutz, A., and Guzzella, L., "Gain-Scheduled Model-Based Feedback Control of the Air/Fuel Ratio in Diesel Engines," *Control Engineering Practice* **17**:1417-1425, 2009.

[8] Jung, M., "Mean-Value Modelling and Robust Control of the Airpath of a Turbocharged Diesel Engine," Ph.D. thesis, Sidney Sussex College, Department of Engineering, University of Cambridge, Cambridge, 2003.

[9] Wei, X. and del Re, L., "Gain Scheduled H_∞ Control for Air Path Systems of Diesel Engines Using LPV Techniques," *IEEE Transactions on Control Systems Technology* **15**(3):406-415, 2007.

[10] Bengea, S., DeCarlo, R., Corless, M., and Rizzoni, G., "A Polytopic System Approach for the Hybrid Control of a Diesel Engine Using VGT/EGR," *Journal of Dynamic Systems, Measurement, and Control* **127**:13-21, 2005.

[11] Stefanopoulou, A. G., Kolmanovsky, I., and Freudenberg, J. S., "Control of Variable Geometry Turbocharged Diesel Engines for Reduced Emissions," *IEEE Transactions on Control Systems Technology* **8**(4):733-745, 2000.

[12] van Nieuwstadt, M. J., Kolmanovsky, I. V., Moraal, P. E., Stefanopoulou, A., and Jankovic, M., "EGR-VGT Control Schemes: Experimental Comparison for a High-Speed Diesel Engine," *IEEE Control Systems Magazine* 63-79, June 2000.

[13] Ferreau, H. J., Ortner, P., Langthaler, P., del Re, L., and Diehl, M., "Predictive Control of a Real-World Diesel Engine Using an Extended Online Active Set Strategy," *Annual Reviews in Control* **31**:293-301, 2007.

[14] Plianos, A., Achir, A., Stobart, R., Langlois, N., and Chafouk, H., "Dynamic Feedback Linearization Based Control Synthesis of the Turbocharged Diesel Engine," presented at the American Control Conference 2007, USA, July 11-13, 2007.

[15] Egardt, B., "Backstepping Control with Integral Action Applied to Air-to-Fuel Ratio Control for a Turbocharged Diesel Engine," presented at SAE World Congress and Exhibition 2002, USA.

[16] Jankovic, M., Jankovic, M., and Kolmanovsky, I., "Constructive Lyapunov Control Design for Turbocharged Diesel Engines," *IEEE Transactions on Control Systems Technology* **8**(2):288-299, 2000.

[17] Chauvin, J., Corde, G., Petit, N., and Rouchon, P., "Motion Planning for Experimental Airpath Control of a Diesel Homogeneous Charge-Compression Ignition Engine," *Control Engineering Practice* **16**, 2008.

[18] Herceg, M., Raff, T., Findeisen, R., and Allgower, F., "Nonlinear Model Predictive Control of a Turbocharged Diesel Engine," presented at 2006 International Conference on Control Applications, Germany, October 4-6, 2006.

[19] Shamdani, A. H., Shamekhi, A. H., and Ziabasharhagh, M., "Air Intake Modelling with Fuzzy AFR Control of a Turbocharged Diesel Engine," *Int. J. Vehicle Systems Modelling and Testing* **3**(1/2), 2008.

[20] Utkin, V. I., Chang, H.-C., Kolmanovsky, I., and Cook, J. A., "Sliding Mode Control for Variable Geometry Turbocharged Diesel Engines," presented at 2000 American Control Conference, USA, June 2000.

[21] Nlwa, S., Kajitani, M., Sagimori, K., and Nakajima, K., "Development of Coordinated Algorithm of EGR and Boost Pressure Based on the Adaptive Sliding Mode Control," SAE Technical Paper 2008-01-0996, 2008.

[22] Chatlatanagulchai, W., Yaovaja, K., Rhienprayoon, S., and Wannatong, K., "Air-Fuel Ratio Regulation with Optimum Throttle Opening in Diesel-Dual-Fuel Engine," SAE Technical Paper 2010-01-1574, 2010.

[23] Chatlatanagulchai, W., Yaovaja, K., Rhienprayoon, S., and Wannatong, K., "Air/Fuel Ratio Control in Diesel-Dual-Fuel Engine by Varying Throttle, EGR Valve, and Total Fuel," SAE Technical Paper 2010-01-2200, 2010.

[24] Chatlatanagulchai, W., Pongpanich, N., Rhienprayoon, S., and Wannatong, K., "Quantitative Feedback Control of Air Path in Diesel-Dual-Fuel Engine," SAE Technical Paper 2010-01-2210, 2010.

[25] Ryan, E. P. and Corless, M., "Ultimate Boundedness and Asymptotic Stability of a Class of Uncertain Dynamical Systems via Continuous and Discontinuous Control," *IMA Journal of Mathematical Control and Information* **1**:223-242, 2008.

[26] Edwards, C. and Spurgeon, S. K., Sliding Mode Control: Theory and Applications, Taylor and Francis, London, ISBN 0-7484-0601-8, 1998.

[27] Utkin, V. I., Sliding Modes in Control Optimization, Springer-Verlag, Berlin, 1992.

[28] Utkin, V., Guldner, J., and Shi J., Sliding Mode Control in Electromechanical Systems, CRC Press, Florida, 1999.

[29] Khalil, H. K., Nonlinear Systems, Prentice Hall, 2001.

CONTACT INFORMATION

Contact Withit Chatlatanagulchai at mailing address:

Department of Mechanical Engineering
Faculty of Engineering
Kasetsart University
50 Phaholyothin Road,
Bangkok 10900, Thailand

or email address: fengwtc@ku.ac.th

ACKNOWLEDGMENTS

We would like to thank Kittipong Yaovaja for performing experiments.